ORIGINAL ARTICLE

**Imran Akhtar · Rajat Mittal · George V. Lauder ·
Elliot Drucker**

Hydrodynamics of a biologically inspired tandem flapping foil configuration

Abstract Numerical simulations have been used to analyze the effect that vortices, shed from one flapping foil, have on the thrust of another flapping foil placed directly downstream. The simulations attempt to model the dorsal–tail fin interaction observed in a swimming bluegill sunfish. The simulations have been carried out using a Cartesian grid method that allows us to simulate flows with complex moving boundaries on stationary Cartesian grids. The simulations indicate that vortex shedding from the upstream (dorsal) fin is indeed capable of increasing the thrust of the downstream (tail) fin significantly. Vortex structures shed by the upstream dorsal fin increase the effective angle-of-attack of the flow seen by the tail fin and initiate the formation of a strong leading edge stall vortex on the downstream fin. This stall vortex convects down the surface of the tail and the low pressure associated with this vortex increases the thrust on the downstream tail fin. However, this thrust augmentation is found to be quite sensitive to the phase relationship between the two flapping fins. The numerical simulations allows us to examine in detail, the underlying physical mechanism for this thrust augmentation.

Keywords Flapping foil · Complex moving boundaries · Thrust augmentation · Fish fins · Fish locomotion

PACS 47.11.–j, 47.63.M–

1 Introduction

Engineers are increasingly looking for inspiration from nature and there is a great interest in making miniature machines that can mimic those that Nature has perfected through millions of years of evolution. Researchers have already built a micro-aerial vehicle of the size of a housefly and several mechanical designs evolved in fish are currently inspiring robotic devices for propulsion and maneuvering purposes in underwater vehicles

I. Akhtar · R. Mittal (✉)
Department of Mechanical and Aerospace Engineering,
The George Washington University, Washington, DC 20052, USA
E-mail: mittal@gwu.edu

Present address:
I. Akhtar
Department of Engineering Science and Mechanics, Virginia Tech., Blacksburg, VA 24061, USA

G. V. Lauder · E. Drucker
Department of Organismic and Evolutionary Biology, Harvard University, Cambridge, MA 02138, USA

Present address:
E. Drucker
Washington Trout, Duvall, WA 98019, USA

[1,2]. One engineered system that could substantially benefit from biological inspiration is the autonomous underwater vehicle (AUV). As research and use of AUVs is expanding [3], there is increased demand for improved efficiency and performance to allow for longer and more complex missions.

Birds and insects use flapping to generate both propulsion and lift. Flapping motion can be viewed as a combined pitching and heaving motion and Knoller and Betz [4–6] were one of the first to explain the mechanism of thrust generation for such flapping foils. Combined pitching and heaving is a motion that also makes an appearance in swimming animals. For instance, the motion of the tail (caudal) fin of most fish can essentially be viewed as a combined pitch-and-heave motion [7]. One key feature that is unique to fish is the presence of multiple sets of fins which allow them to propel and maneuver precisely in aquatic environments that are usually highly unsteady. For instance, many species of fish have highly developed dorsal, pectoral, pelvic, anal and caudal fins and the fish can choose to employ one or more of these fins at any given time. This suggests the interesting possibility that a downstream fin might find itself immersed in the flow disturbed by another upstream fin, and that fishes might gain some hydrodynamical advantage from such an interaction. There have been other studies that have examined the effect of upstream vortices on the performance of flapping foils. Several theoretical studies have emphasized the potential for wake interaction among nearby fish fins to increase propulsive efficiency [7–10]. Gopalkrishnan et al. [11] have examined the interaction of a flapping foil with vortices shed by a bluff body. In their experiments, a foil was placed in the wake of a D-section cylinder, sufficiently far behind the cylinder so that it did not interfere with the vortex formation process. The foil performed combined heaving and pitching oscillations at a frequency close to the Strouhal frequency of the cylinder, while the cylinder and foil also moved forward at a constant speed. Flow visualization experiments were conducted at a Reynolds number (Re) of 550 and force and torque measurements were made at a Reynolds number of 20000. By varying the phase of the foil oscillation (varying the spacing between D-cylinder and foil), three basic interaction modes were identified: expanding wake, destructive interaction with cylinder wake and constructive interaction with cylinder wake. They also observed a variation in the propulsive efficiency as a function of spacing between cylinder and foil.

Tuncer and Platzer [12] have studied the thrust generation by a single flapping airfoil and a flapping/ stationary airfoil in tandem. In their simulations, they observed that a flapping airfoil undergoing heave motion produces thrust. In flapping/stationary airfoil analysis, they have studied the effect of a heaving airfoil over a stationary airfoil placed downstream in its wake and observed a significant augmentation of thrust in the latter case. Liao et al. [13] have performed experiments on rainbow trout *Oncorhynchus mykiss* and studied the gait of the trout in the wake of a D-cylinder. The experimental results show that the trout voluntarily alter their body kinematics when interacting with vortices present in the environment that are not self-generated. Their results suggest that fish can capture energy from vortices generated by the environment to maintain station in downstream flow.

Recently Drucker and Lauder [14–16] have performed several experiments with bluegill sunfish, *Lepomis macrochirus* (see Fig. 1). In their experiments, they have used digital particle image velocimetry (DPIV) in order to visualize the wake structures behind fins and to calculate locomotor forces produced by these fins as sunfish swim at speeds of 0.5 and 1.1 total body lengths per second (BL). In one of their experiments [16], they have studied the effect of the presence of the dorsal fin on the thrust and efficiency of the tail fin, and this experiment is of major significance to the current study. Moreover, they have also examined the hydrodynamic impact of the vortices produced by the dorsal fin on the tail fin and the vortices generated by the tail fin itself. Figure 2 shows four video images of the two fins within a frontal plane laser sheet (Fig. 1d, position 2) over the course of one complete stroke cycle during steady swimming. In their paper, they have hypothesized that the presence of dorsal fin upstream of the tail fin could augment the thrust and propulsive efficiency.

In this paper, we examine this hypothesis by modeling the interaction of the dorsal fin with the tail fin through numerical simulations. In order to investigate this effect, it is useful to first study the situation where the dorsal fin is not present upstream of the tail. This could be attempted in experiments by ablating the dorsal fin from a fish, but such a procedure could possibly alter the natural gait of the fish. On the other hand, in a computational model, it is possible to simulate the flow past a tail fin with no upstream dorsal fin and study its thrust and efficiency. Subsequent simulations of the tail fin with an upstream dorsal fin allow us to clearly assess the effect of the dorsal fin on the tail fin performance.

2 Computational modeling

Combined pitch and heave is the primary fin motion through which birds, insects and fish produce the thrust and lift required for motion. The experiment of Drucker and Lauder [16] indicates that the dorsal and tail fin
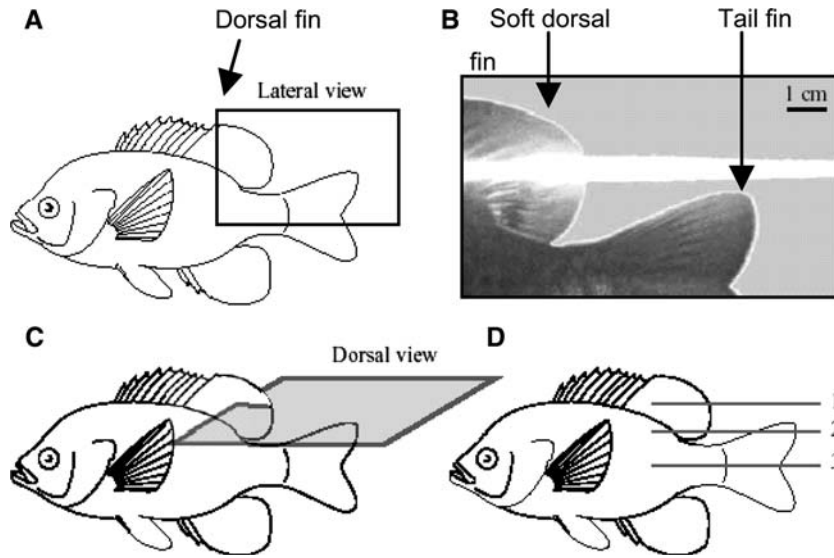
Fig. 1 Overview of the experiment by Drucker and Lauder [16]. Side view of bluegill sunfish is shown indicating: **a** lateral view of the dorsal and tail fins studied here; **b** side-view image of the sunfish dorsal and caudal fins showing the laser-sheet plane intersecting the dorsal fin during DPIV; **c** dorso-lateral view of the laser light sheet plane behind the dorsal fin, imaged from the above with high-speed video; **d** three planes are shown and data discussed in this paper are extracted from plane 2
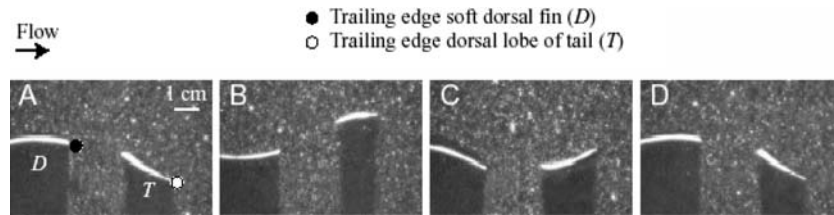

Fig. 2 *Top view* (looking down on the dorsal and tail fins) of bluegill sunfish swimming during DPIV experiments. Plane 2 (see Fig. 1d) showing the dorsal (*D*) and tail (*T*) fin motion over a complete stroke cycle in four video frames **a**–**d** [16]

motion of the bluegill sunfish can also be well approximated as a combined pitch and heave motion. A foil in a steady forward motion and a combination of harmonic heaving and pitching motion produces thrust through the formation of a flow downstream from the trailing edge (TE), which, when averaged over one period of oscillation, has the form of a jet. The pitch and heave motions have the following form:

$$\text{Pitch:} \quad \theta(t) = \theta_{\max} \sin(\omega t + \psi) \tag{1}$$

$$\text{Heave:} \quad y(t) = y_0 + A \sin(\omega t) \tag{2}$$

The non-dimensional fin parameters for single and tandem foil configurations estimated from the experimental data [16] are defined in Table 1. Our analysis shows that the phase-angle ψ between pitch and heave, which has been shown to affect the foil performance [28–30], is close to 90° for both fins. Examination of the experimental data also indicates that the dorsal fin leads tail fin by about 108° in phase. For this specific case, the dorsal and the tail fins can, therefore, be modeled as two foils arranged in tandem (see Fig. 3b) undergoing pitch and heave motion with a phase difference of 108° between them. For the sake of simplicity, we model the foil shapes as finite-thickness flat plates with rounded leading and trailing edges. There are obvious limitations of the current computational model in terms of the simplifications that have been assumed with regards to the fin geometry and kinematics. The fish body and fins are three-dimensional whereas the current study is two-dimensional. Furthermore, the fish fins are relatively flexible but here we employ rigid flapping foils. However, despite these limitations of the computational modeling, it is expected that the results of the analysis would lead to some useful insights regarding the dorsal–tail fin interaction and more importantly, guide us towards bio-inspired flapping foil propulsors that have high performance. The Reynolds number during the experiment is about 5,000, which requires a very high resolution grid for the numerical simulations. Due to

Table 1 Fin non-dimensional parameters used in tandem flapping foil numerical simulations

Parameter	Dorsal fin (d)	Tail fin (t)
Amplitude to chord ratio (A/c)	0.32	0.56
Thickness ratio (t/c)	1/12	1/8
Maximum pitch angle (θ_{max})	$\approx 20°$	$\approx 30°$
Phase angle between pitch and heave (ψ)	90°	90°
Reynolds number, $Re = U_\infty c/\nu$	630	600
Strouhal number, $St = f2A/U_\infty$	0.19	0.28
Chord ratio (c_d/c_t)	1.058	–
Mean distance between fins (l/c_t)	0.996	–
Phase difference (ϕ) between fins	108°	–

Parameters were measured from high-speed video images of dorsal and tail fin movement from the study of Drucker and Lauder [16]. Parameters are defined in Fig. 3. All lengths are normalized by the tail-fin chord-length (c_t)
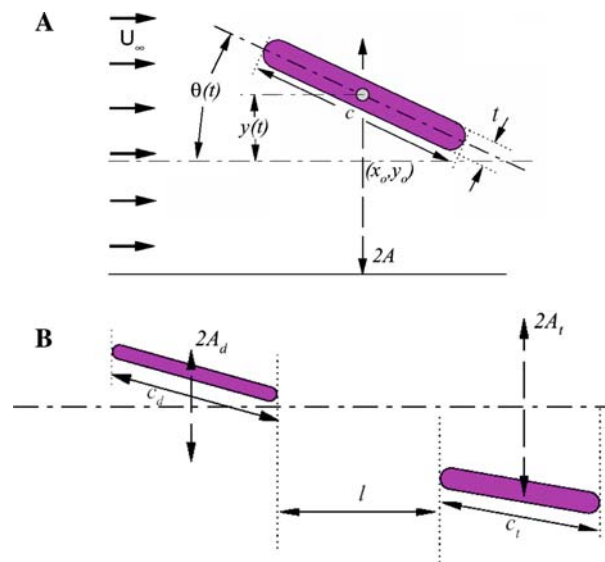
Fig. 3 Schematic of **a** tail-fin only **b** tandem-fin arrangement indicating various parameters used in the current study

this, the numerical simulations were carried out at a Reynolds number of 600 to limit the grid requirements and obtain grid independent results. Past studies [3] have shown that thrust performance of flapping foils is relatively insensitive to Reynolds number. It should, however, be pointed out that the Strouhal number (St), which is a key parameter for the flapping foils [21], is matched between the simulations and experiment.

3 Numerical method

A Cartesian grid solver [17,18] is employed in these simulations. The advantage of this method is that the complexity and cost of generating a body-conformal mesh at each time-step is eliminated, thereby easing the resources required to perform such simulations. The framework of the method developed in these papers is Eulerian–Lagrangian, i.e., the immersed boundaries are explicitly tracked as curves in Lagrangian fashion, while the flow computations are performed on a fixed Eulerian mesh. This affords the advantage of pure Lagrangian methods such as explicit interface information without ambiguities associated with a posteriori reconstruction of the interface from an advected scalar (such as volume-of-fluid (VOF) and level set [19]). In contrast with purely Eulerian-interface-capturing approaches (diffuse interface methods), the current method treats the immersed boundaries as sharp interfaces [20]. The distinguishing feature of the present method is that the governing equations are discretized on a Cartesian grid, which does not conform to the immersed boundaries. This greatly simplifies grid generation and also retains the relative simplicity of the governing equations in Cartesian coordinates. Therefore, this method has distinct advantages over the conventional body-fitted approach in simulating flows with moving boundaries, complicated shapes or topological changes.
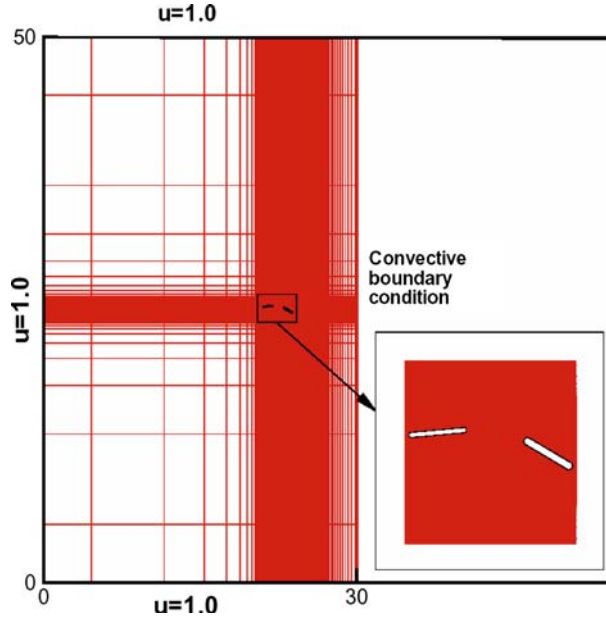
Fig. 4 Typical non-uniform grid and boundary conditions used for this study. A magnified view of the fine mesh region with the tandem-fin arrangement is also shown

The fractional step scheme is used for advancing the solution in time. The Navier–Stokes equations are discretized on a Cartesian mesh using a cell-centered collocated (non-staggered) arrangement of the primitive variables $\vec{u}$ and p. The integral forms of the non-dimensionalized governing equations are used as the starting point:

$$\oint \vec{u} \cdot \vec{n} \, \mathrm{d}S = 0 \tag{3}$$

$$St \frac{\partial}{\partial t} \oint \vec{u} \, \mathrm{d}V + \oint \vec{u}(\vec{u}.\vec{n}) \, \mathrm{d}S = - \oint p\vec{n} \, \mathrm{d}S + \frac{1}{Re} \oint \nabla \vec{u}.\vec{n} \, \mathrm{d}S \tag{4}$$

where $\vec{u}$ is non-dimensional velocity vector, p is pressure and $\vec{n}$ is a unit vector normal the face of the control volume. The above equations are to be solved with $\vec{u}(\vec{x}, t) = \vec{u}_\partial(\vec{x}, t)$ on the boundary of the flow domain where $\vec{u}_\partial(\vec{x}, t)$ is the prescribed boundary velocity, including that at the immersed boundary. A non-uniform Cartesian grid is employed to carry out the analysis as shown in Fig. 4. The mesh size is 520×240 and the domain size chosen is 30×50. The mesh is divided into nine domains wherein the center domain, which surrounds the two foils, has a uniform 300×180 grid. Outside this core region, the mesh is stretched in all directions but the mesh-stretching factor in the wake region is kept below 2%, in order to limit dispersion errors and provide adequate resolution of the wake vortex structure.

4 Results

Numerical simulations have been carried out in order to understand the effect of the dorsal fin on the tail fin. The results of the tandem fin/foil simulations are compared to one with a single fin model of the tail fin by just removing the upstream dorsal fin. Thus there are two distinct cases:

(a) Tail-fin only case: Only the tail fin is modeled as a flapping foil.
(b) Tandem-fin arrangement: Both the dorsal and tail fins are modeled as a tandem flapping foil configuration where the upstream dorsal fin leads the tail fin by 108° in phase.

4.1 Performance of a pitching–heaving foil

In the analysis of the performance of an oscillating foil, the key performance factors are thrust and efficiency [11,21]. Considering the rounded plate, as shown in Fig. 3a, the fin is subjected to time varying forces $T(t)$, $S(t)$ in the x-(forward) and y-(transverse, or lift) directions, respectively; and a torque $M(t)$ about its center. The forces and moments on the foils are computed by numerically integrating the pressure and shear stresses on the surfaces of the foils. For any general function $f(t)$, the average over N cycles is defined as

$$\langle f \rangle = \frac{1}{N\tau} \int_0^{N\tau} f(t)\,\mathrm{d}t \tag{5}$$

where τ is the time period of oscillating tail fin. Thus, the average thrust coefficient (C_T), transverse coefficient (C_S) and moment coefficient (C_M) are defined as

$$C_T = \frac{\langle T \rangle}{\frac{1}{2}\rho U^2 c_t} \tag{6}$$

$$C_S = \frac{\langle S \rangle}{\frac{1}{2}\rho U^2 c_t} \tag{7}$$

$$C_M = \frac{\langle M \rangle}{\frac{1}{2}\rho U^2 c_t^2} \tag{8}$$

respectively, where ρ denotes the fluid density and c_t is the chord length of the tail fin. Furthermore, the propulsive efficiency (η_P) is defined as the ratio of useful power to input power (P) [21].

$$\eta_P = \frac{\langle TU \rangle}{P} = \frac{\langle T \rangle U}{P} \tag{9}$$

where

$$P = \langle S \cdot \dot{y} \rangle + \langle M \cdot \dot{\theta} \rangle \tag{10}$$

4.2 Grid and domain dependence

Grid and domain independence studies are critical in order to verify the accuracy of the computation results. Therefore a study has been carried out to verify the grid/domain independence of the simulation results of tail fin with 108° phase difference with the dorsal fin. The grid size being used for the numerical simulations is 520×240 with a grid of 300×180 in the core fine mesh region. In order to check the dependence on grid size, the grid size was increased to 700×430 where the grid in the core region was increased to 580×350. Thus, the grid resolution in the core region was increased by more than 90%. The results from the two simulations are given in Table 2. It is observed that the percentage difference for the thrust and lift forces is less than 5%, which clearly indicates that the flow in the vicinity of the foils is virtually grid independent.

The domain size being used for the numerical simulations is 30×50 with grid size of 520×240. In order to check for domain dependence, the domain size was increased to 40×60 with grid size of 577×262. The slight increase in the grid size on the larger domain was done in order to maintain comparable grid spacing in the two grids. The numerical simulation results are given in Table 3 and indicate that the domain size of 30×50 is quite adequate for the current study.

Table 2 Grid dependence study carried out for tandem-fin arrangement

Parameter	Dorsal fin		Tail fin	
	520×240	700×430	520×240	700×430
Total mean thrust	−0.0545	−0.0569	0.2719	0.2733
Total rms thrust	0.0531	0.0511	0.2574	0.2539
Total rms lift	0.4147	0.4146	1.4037	1.3831

Table 3 Domain dependence study carried out for tandem-fin arrangement

Parameter	Dorsal fin		Tail fin	
	30×50	40×60	30×50	40×60
Total mean thrust	−0.0545	−0.0559	0.2719	0.2697
Total rms thrust	0.0531	0.0532	0.2574	0.2545
Total rms lift	0.4147	0.4163	1.4037	1.3759

(a) Tail-fin only case   **(b)** Tandem-fin arrangement
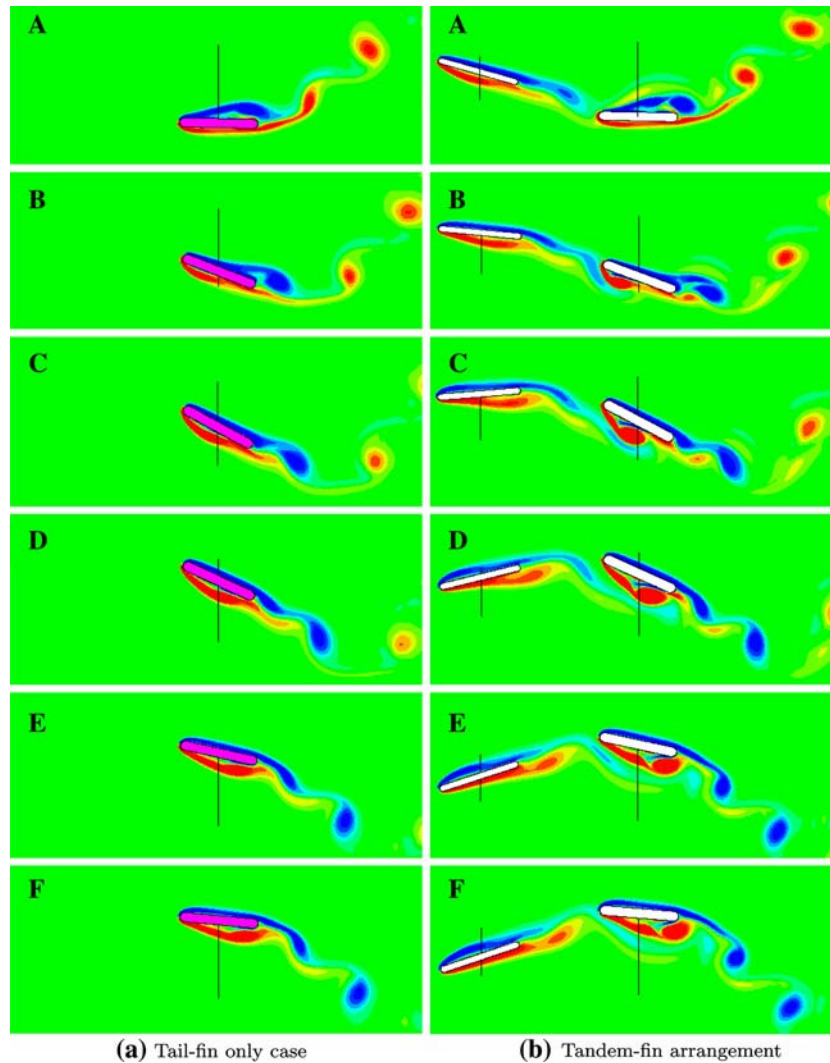
Fig. 5 Spanwise vorticity contours plotted over a half fin beat cycle for two cases: **a** tail-fin only case (*A–F*), and **b** tandem-fin arrangement (*A–F*), showing six various locations of the tail fin along the vertical line indicating peak–peak amplitude. All plots show the same range of contours values for comparison

4.3 Simulation results

Figure 5a, b shows spanwise vorticity contours during one half cycle, of the tail-fin only case and tandem-fin arrangement respectively, in which the fin moves from the bottom-most position (A) to the top-most position (F). The blue (dark) and red (light) contours represent clockwise and counterclockwise values of vorticity, respectively. Figure 5a-A shows the tail fin at the bottom of its cycle and as the fin moves up, the pitch angle increases and a clockwise vortex that was created on the top of the tail fin during the previous downward stroke is about to convect into the wake (see Fig. 5a-B). In Fig. 5a-C, the tail fin reaches the halfway point in

its upward trajectory and is at its maximum pitch angle of 30°. At this point, we observe that the boundary layer on the lower surface that has detached from the leading edge (LE) reattaches to the foil near the TE. As the foil moves up further, the pitch angle starts decreasing as shown in Fig. 5a-D. At this point, the boundary layer on the top surface, which detaches at the TE, rolls into another distinct clockwise vortex and seems to shed into the wake. The detached boundary layer on the lower surface rolls up into a small counter clockwise vortex near the TE of the fin. This vortex later detaches from the foil and convects into the wake similar to the clockwise vortex in the previous half cycle. Thus in each cycle, two clockwise and two counter-clockwise vortices are shed in the wake.

Spanwise vorticity contours for the 108° phase tandem-fin arrangement, at the same instant as that of tail-fin only case, are shown in order to facilitate a direct comparison. Although there are many similarities between the two cases, the plots in Fig. 5b clearly show the interaction of the wake from the upstream fin colliding with the LE of the tail fin. One key feature that seems to be different between the two cases is that the the detached shear layer on the lower side of the foil forms a very distinct and relatively large counter-clockwise vortex which convects along the lower surface of the fin until it convects downstream into the wake. We will examine this feature in detail in the following discussion.

Figure 6 shows four distinct phases of the tail fin during its motion which are used to facilitate the discussion of the results. In Fig. 7, heave velocity and pitch are plotted for different positions of the tail fin at various instants. It is clear that when the fin is at the center position, its heave (vertical) velocity and pitch
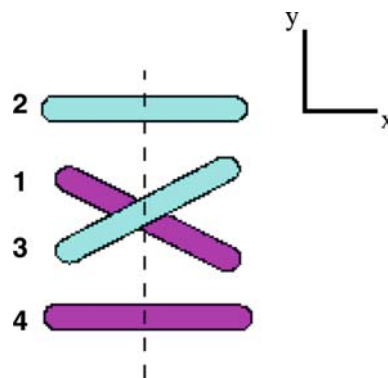

Fig. 6 Position of the tail fin at different phases over a complete flapping cycle: *1* center position (moving up), *2* top position, *3* center position (moving down), and *4* bottom position
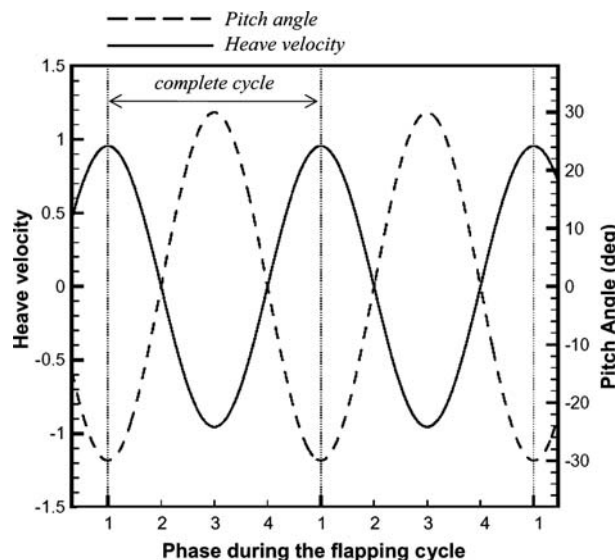

Fig. 7 Time variation of heave velocity (chord lengths/s) and pitch angle over two flapping cycles of the tail fin. *x*-axis corresponds to phases shown in Fig. 6
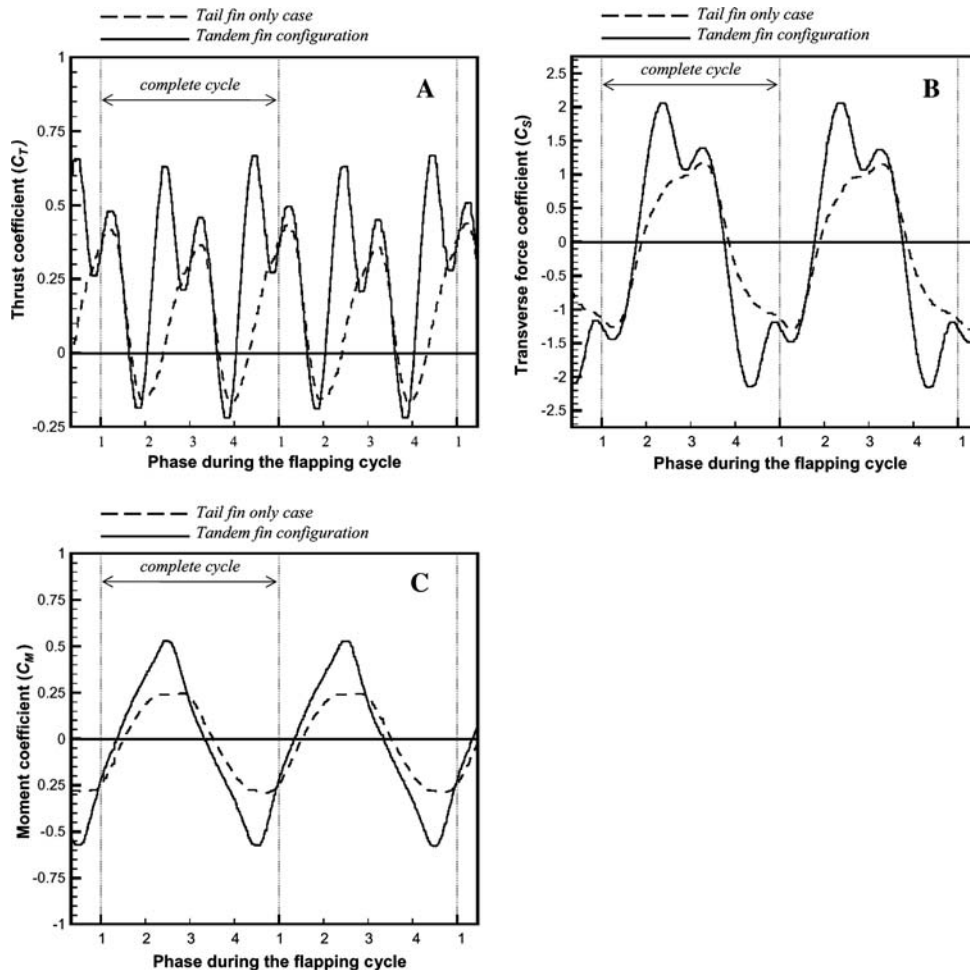
Fig. 8 Time variation of performance parameters plotted over two flapping cycles. **a** Mean thrust coefficient, **b** transverse force coefficient and **c** moment coefficient compared for tail-fin only case and tandem-fin arrangement corresponding to phase difference (ϕ) of 108° between dorsal and tail fin from experiment of Drucker and Lauder [16]. *x*-axis corresponds to phases shown in Fig. 6

angle are at peak values and are minimum at the two extreme positions. Although we have simulated over ten cycles for each case, we present here data for two complete cycles only. The thrust, transverse force and moment coefficients experienced by the fin are plotted against time in Fig. 8 for comparison of the two cases (tail-fin only and tandem-fin arrangement). The temporal variation of the thrust coefficient for both cases are plotted in Fig. 8a. Different phases, corresponding to Fig. 6, of the tail fin are marked on the abscissa and thrust coefficient is plotted on the ordinate. It is observed that there is a significant increase in the thrust of the tail fin due to the presence of the dorsal fin, primarily during the phase when the foil accelerates towards its mid-position from either of the two ends of its trajectory. A similar comparison of the transverse forces is shown in Fig. 8b. As expected, the transverse force is equal in magnitude but opposite in direction for the two halves of a complete cycle. The plot of moment coefficient against time is shown in Fig. 8c and the moment coefficient is also symmetric for the two halves of a cycle. Comparison of pressure coefficients of the two cases by Akhtar [22] at different phases of the tail fin motion indicates the formation of a larger counter-clockwise vortex in tandem-fin arrangement convecting down the suction side.

The magnitude of mean thrust and efficiency of the tail fin for both cases have been computed and are presented in Table 4. A comparison between the two cases shows that the presence of the upstream fin increased the thrust of the tail fin by about 107% and the efficiency by about 52%. The numerical simulations therefore clearly indicate that the presence of the upstream fin can greatly increase the thrust and efficiency of the tail fin. This provides some confirmation of the hypothesis of Drucker and Lauder [14] that the vortex structures shed from the dorsal fin could enhance the performance of the tail fin. However, for the results of this study

Table 4 Comparison of thrust coefficient and efficiency between tail-fin only and tandem-fin arrangement with 108° phase difference

Parameter	Tail-fin only case	Tandem-fin arrangement	% change
Mean thrust coefficient (C_T)	0.128	0.272	+107
Efficiency (η_P)	0.172	0.261	+52
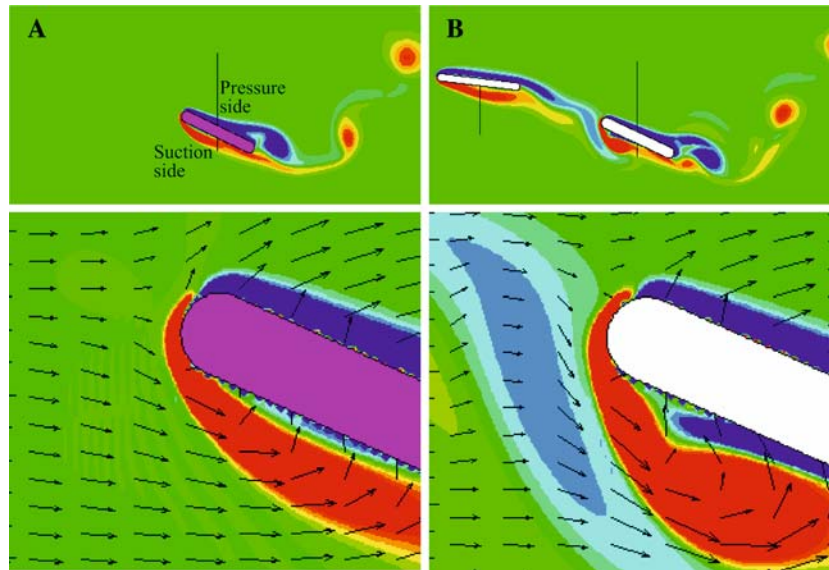
Fig. 9 Spanwise vorticity contours near the leading edge of the tail fin for the two cases at the time instant corresponding to Fig. 5 position **b**. **a** Tail-fin only case and **b** tandem-fin arrangement with the phase difference of 108° plotted side by side for direct comparison. Both plots show the same range of contours values for comparison. Also plotted is the close-up view of the leading edge vortex of the tail fin for each case with the velocity vectors. (Note that only every sixth vector is plotted in each dimension)

to be useful, it is essential to explain the physical mechanism(s) that is (are) responsible for this performance enhancement, and determine what is(are) the key factor(s) causing this enhancement. Understanding of the underlying mechanisms could eventually allow us to eventually develop bio-inspired flapping-foil propulsors.

In Fig. 9, we have plotted flow visualizations for the two cases at a point where the tail fin is halfway between the bottom (phase 4 of Fig. 6) and center (phase 1 of Fig. 6) points in its trajectory and moving up. This is approximately the phase where tail-fin in the tandem-fin arrangement produces significantly more thrust than the tail-fin only case (see Fig. 8a). Thus examination of the flow at this phase should allow us to gain insight into the key difference between the two flows. A zoomed-in view of the flow near the tail-fin LE is also shown in Fig. 9 along with velocity vectors and a number of interesting features can be observed. First, at this phase, tail-fin only case shows flow separation at the LE of the tail-fin. However, the separation is quite marginal and the flow quickly reattaches to the lower surface of the foil. This separation is a result of the negative effective angle-of-attack that is seen by the tail fin as it heaves upwards while simultaneously pitching up about its center. Nominally, this angle-of-attack at any time instant is given by $\alpha(t) = \theta(t) - \frac{\dot{y}(t)+0.5c\times\dot{\theta}(t)}{U_\infty}$ which at this phase is equal to 38°. However at this phase, for tandem-fin arrangement, a clockwise rotating vortex from the dorsal fin is seen approaching the LE of the tail-fin and the velocity vectors indicate that this tends to increase effective angle-of-attack of the tail-fin at this phase. This increase in effective angle-of-attack leads to a more noticeable LE separation and subsequent destabilization of the separated shear layer thus causing the formation of a distinct LE stall vortex as clearly seen in Fig. 9. Figure 10 shows the variation of pressure coefficient (C_P) on the pressure (upper) and suction (bottom) surfaces of the tail-fin at this phase. This plot clearly shows that the presence of the LE stall vortex in tandem-fin arrangement results in a significant higher suction pressure (in the region from the LE to about 30% x/c) on the lower surface and given the orientation of the tail fin at this phase, this leads to an increase in thrust. Note that this triggering of a LE stall vortex due to an upstream wake vortex is distinct from any of the three mechanisms proposed by Gopalakrishnan et al.
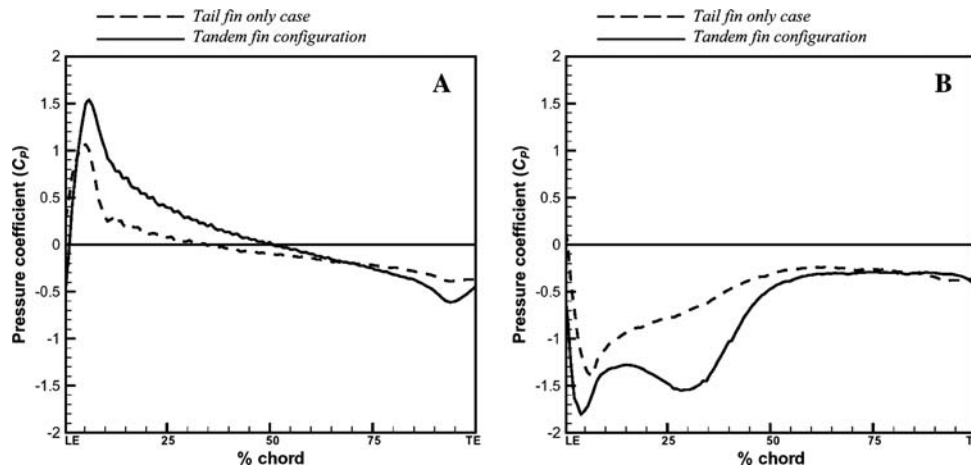
Fig. 10 Pressure coefficient (C_P) distribution on the tail fin for the two cases at the time instant corresponding to Fig. 9. Pressure coefficient plotted from LE (leading edge) to TE (trailing edge) over **a** pressure side and **b** suction side. Tandem-fin arrangement corresponds to phase difference (ϕ) of 108° from experiment [16]

[11] and represents potentially, an entirely new mechanism of vorticity control that is employed by swimming animals.

4.4 Phase difference study

Analysis of the vortex structures indicates that the physics of thrust enhancement is associated with the interaction of a clockwise rotating vortex with the LE of the tail fin as it moves up (and vice-versa). It seems clear that the phase-lag between the two fins would be a crucial factor since it would determine the timing of the interaction between the dorsal fin vortices and the tail fin LE. Thus, it seems evident that an examination of the effect of the phase difference between the two fins would lead to further insight into the physics of this flow. The particular phase-lag between the dorsal and tail fin in this case is a result of various constraints that are specific to bluegill sunfish as well as the particular individual fish examined here. For instance, the phase-lag is clearly a function of the distance between the dorsal and tail fin as well as the speed of the body-wave that actuates both the dorsal and tail fins as well as the activity of intrinsic muscles controlling the fins themselves [23,24]. Fish of different sizes would likely also have different phase relationships between the two fins. Examination of the effect of phase-lag on the thrust performance is also of interest from the point of view of developing tandem flapping foil propulsors inspired by this mechanism since these tandem configurations would not necessarily be subject to the same constraints that a fish is subject to.

Numerical simulations were therefore carried out assuming different phase lags between the two fins. With the dorsal fin still leading, phase differences of 138°, 123°, 108°, 93°, 78°, 63°, 48°, 33° and 18° were used at the same Reynolds number. Figure 11 shows the vorticity plots for five different phase lags, along with the original 108° phase difference, when the tail fin is at its mean position with maximum pitch angle. A comparison of these plots yields some interesting observations. First, all cases show the rollup of the vorticity layer on the lower surface to an extent that is more than that for the tail-fin only case. Thus, it seems that for all phase-difference, the upstream wake tends to destabilize the separated vorticity layer on the tail-fin LE. The rollup is generally found to be most noticeable for the lower phase-difference, where as for 138° and 123° phase-lag cases, the rolled up vortex is clearly smaller than the other cases. Also, it can be clearly seen that for the largest phase-difference of 138°, the vortices from the dorsal fin also impact the boundary layer on the upper side of the tail fin and form distinct vortices that convect down this surface. It should also be pointed out that although for the lower phase-difference (for instance 48°), it does not seem that the upstream wake interacts directly with the tail-fin, in fact, this interaction just occurs earlier in the upward motion of the tail-fin.

Figure 12 shows a plot of the thrust coefficient of the tail fin versus phase angle. On the right ordinate, the thrust on the tail-fin with upstream dorsal fin normalized by the thrust of the tail-fin only case is plotted. This gives us a direct measure of the tail fin thrust enhancement due to the presence of the dorsal fin. The circled value indicates the phase difference of 108°, which was based on the initial experimental value and for which the thrust is almost twice that of tail-fin only case. It is interesting to see that as the phase difference between
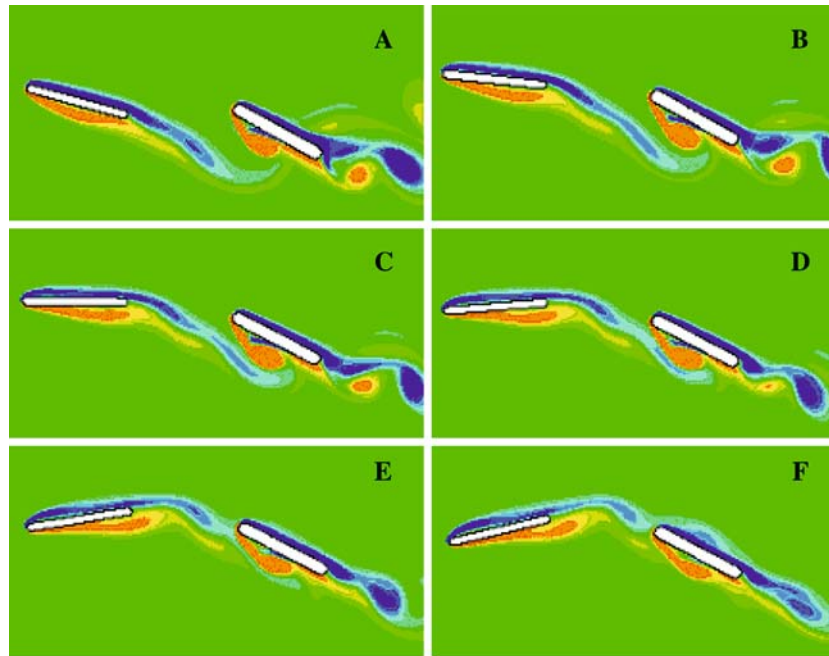
Fig. 11 Spanwise vorticity contours plotted at the time instant when the tail fin is at its center during upward motion (phase 1 in Fig. 6). Tandem-fin arrangement analyzed over various phase differences (ϕ) corresponding to **a** 48°, **b** 78°, **c** 93°, **d** 108°, **e** 123° and **f** 138° and plotted side by side for direct comparison. All plots show the same range of contours values for comparison
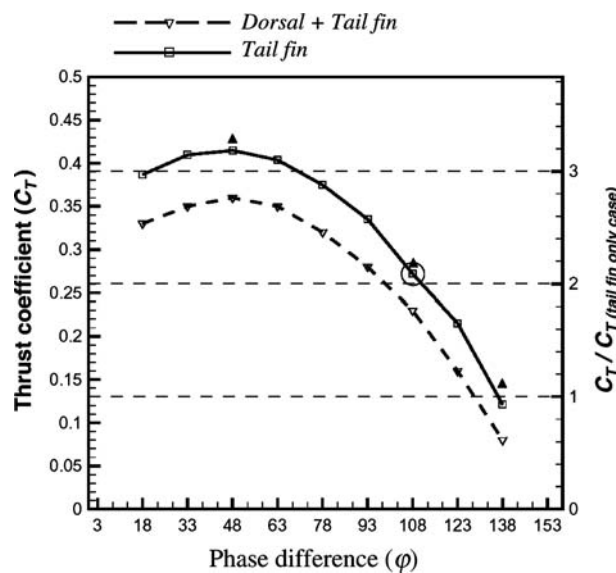

Fig. 12 Mean thrust coefficient on the tail fin (*left y*-axis) plotted for entire range of phase difference studied in tandem-fin arrangement. Mean thrust coefficient normalized with respect to the tail-fin only CASE (*right y*-axis) to compare thrust augmentation. "Dorsal + Tail fin" curve shows the total thrust of both fins while "Tail fin" curve shows thrust for the tail fin in the tandem-fin arrangement system. *Circled phase* corresponds to $\phi = 108°$ from the experiment and *filled triangles* correspond to thrust coefficients for the tail fin in the tandem-fin configuration at $Re = 1200$

the dorsal and the tail fins is increased to 123°, the thrust starts to decrease but is still greater than for tail-fin only case. However, as the phase difference is increased further, the thrust decreases to a value slightly lower than that of tail-fin only case. On the other hand, decreasing the phase difference causes the thrust to increase up to a phase difference 48° where maximum thrust enhancement is achieved. At this point, the thrust is just
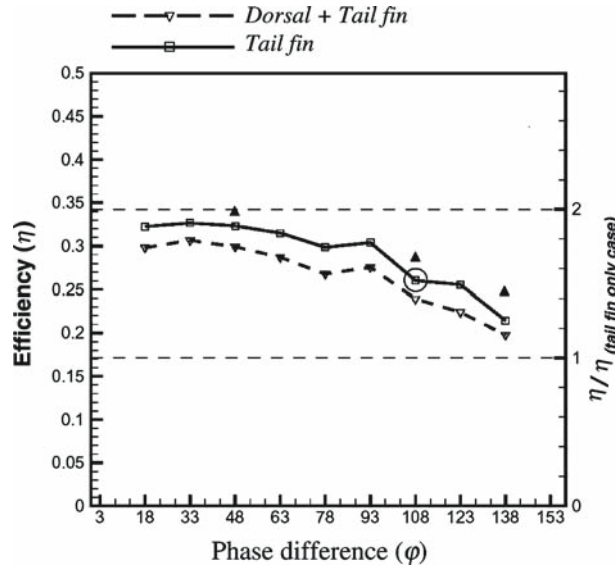
Fig. 13 Efficiency (*left* y-axis) plotted for entire range of phase differences studied for the tandem-fin arrangement. Efficiency normalized w.r.t tail-fin only case (*right* y-axis) to compare efficiency augmentation. "Dorsal + Tail fin" plot shows total efficiency of both fins while the "Tail fin" plot shows the efficiency of the tail fin in the entire tandem-fin arrangement. Circled phase corresponds to $\phi = 108°$ from the experiment on sunfish and filled triangles correspond to efficiencies for the tail fin in the tandem-fin configuration at $Re = 1200$

over three times the thrust of the tail-fin only case! With further decrease in the phase difference, the thrust tends to reduce slowly from this peak value.

Figure 13 shows the variation of efficiency of the tail fin. The phase difference of 108° is again circled and for this case, as noted before, there is a 50% increase in efficiency. As the phase difference is increased, the efficiency goes down, but even for the largest phase difference of 138°, the efficiency is about 20% larger than that of tail-fin only case. As the phase difference is reduced the efficiency is found to increase and reaches a broad maximum at a phase difference of about 33°. At this phase difference, the efficiency is almost 90% more than that of tail-fin only case. Efficiency values are of nearly the same magnitude for phase difference of 33° and 18°. Thus at these lower phase differences, we get an amazing threefold increase in thrust and a nearly twofold increase in efficiency!

As on an airfoil, lift and drag/thrust is produced primarily due to the pressure differential across the pressure and suction sides of the airfoil since shear stress is of a significantly lower magnitude. It is, therefore, useful to examine the surface pressure distribution for some key cases. Here we compute the local force coefficient per unit area due to pressure into its thrust x-component as follows:

$$C_{px} = -n_x C_p \tag{11}$$

where n_x is the x component of the local unit normal. In addition to the tail-fin only and 108° phase cases, cases with 48° and 138° phase difference are also chosen for comparison since they lie at the two extremes of the chosen ranges. In Fig. 14a, we plot C_{px} on the pressure (upper) side of the tail fin for position shown in Fig. 9. Note that negative values of C_{px} correspond to positive thrust and vice versa. All the four cases, show similar behavior on the pressure side of the tail fin. In Fig. 14b, we plot on the suction (bottom) side of the tail fin for position shown in Fig. 9. We note from the figures that there is a distinct suction peak in all the cases at the LE at around $x/c = 5\%$ which is due to the acceleration of the flow over the LE. This peak is smallest for the 138° phase difference case and largest for the 48° phase difference case. The peak for the tail-fin only case is approximately midway between these two cases. Thus a significant part of the thrust augmentation occurs due to the modification in the flow around the LE of the tail-fin. In addition, there is secondary smaller but broader peak for the 48° and 108° phase difference cases at about $x/c = 35\%$ which is due to the rolled up leading-edge stall vortex. No such peak is visible for the tail-fin only and 138° phase difference cases and this is the second component of the thrust augmentation. Thus, the examination of phase difference clearly indicates that thrust-augmentation is connected to increased suction at the LE as well as the formation of distinct and relatively large stall-vortex induced by the upstream wake vortices.
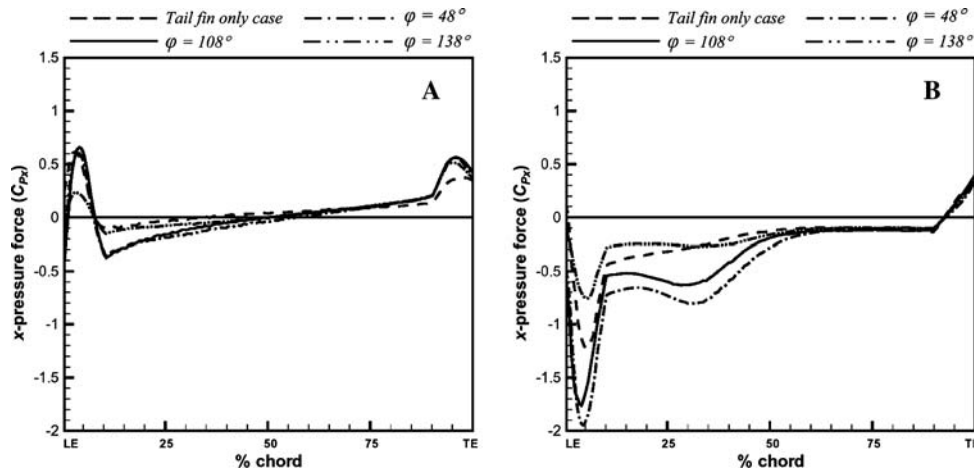
Fig. 14 x-pressure force component over tail fin plotted for the tail-fin only case and tandem-fin arrangement at the time instant shown in Fig. 11. x-pressure force component plotted from LE to TE over **a** pressure side and **b** suction side. Three phase differences ($\phi = 48°$, $108°$ and $138°$) corresponding to maximum thrust/efficiency, experimental data, and minimum thrust/efficiency respectively are compared with tail-fin only case to study thrust augmentation

A set of simulations have also been carried out at a Reynolds number of 1,200, which is twice the current value of 600. The objective here is to examine the sensitivity of the observed behavior to the Reynolds number. These simulations have been carried out on a finer 700×430 grid, and due to the larger computational effort required for these simulations, we have limited the study to three phase-angles of 48°, 108° and 138°. The thrust coefficient and efficiency values for these cases are also plotted in Figs. 12 and 13, respectively. The thrust coefficient of the tail for the tail-only case increases slightly to a value of 0.17, and this is attributed, to some extent, to lower shear drag at the higher Reynolds number but mainly due to increase in the strength of the LE vortex and corresponding surface pressure. For the tandem configuration, the thrust-coefficient for the tail-fin follows a trend with phase-angle that is very much in line with that observed for the $Re = 600$ case. Similarly, the baseline efficiency of the tail-only case goes up to a value of 0.24 but the trend for the tandem configuration is very much inline with that for the $Re = 600$ case. Thus, even a doubling of the Reynolds number does not modify the overall trend, thereby confirming the relative insensitivity of the underlying physical mechanisms to this parameter.

4.5 Overall efficiency of tandem foil configuration

In the previous sections, the thrust and efficiency of the tail fin have been discussed with or without the presence of upstream dorsal fin. In both cases, we discussed the hydrodynamic performance of the tail-fin only. However, in case of the tandem-fin arrangement, it is logical to ask how well the entire tandem-fin arrangement performs compared to the tail-fin-only case. This question is particularly relevant when considering such a propulsive system for an underwater vehicle. We, therefore, consider the thrust and efficiency of the entire tandem-fin arrangement and compare that to the tail-fin only case. Thus the efficiency of the tandem-fin arrangement is calculated as

$$\eta_P = \frac{(\langle T_{\text{dorsal}} \rangle + \langle T_{\text{tail}} \rangle) U_\infty}{P_{\text{dorsal}} + P_{\text{tail}}} \tag{12}$$

The thrust and efficiency of the tandem-fin arrangement is also plotted in Figs. 12 and 13. We note that there is a slight decrease in the overall thrust, and this is due to the small amount of drag produced by the dorsal fin. However, the overall thrust is still higher than the thrust of the tail-fin only case for most of the phase angles. In fact, for the 48° phase difference case, the overall thrust of the tandem-fin arrangement is still a factor of 2.7 higher than the tail-fin-only case. Thus, the thrust of the dorsal–tail fin combination is significantly more than what would be produced even by two tail-fins operating independently. The efficiency for the dorsal–tail fin combination is also somewhat lower than the value computes for the tail-fin due to the drag and the power consumption of the dorsal fin. However, despite this, the peak efficiency of the combination is still about a

factor of 1.8 higher than the tail-fin only case. Thus, both in terms of thrust and efficiency, the tandem-fin arrangement far outperforms the tail-fin only case.

5 Conclusions

Two-dimensional numerical simulations have been used to examine the performance of a foil undergoing flapping motion in the wake of another flapping foil. This configuration attempts to mimic the interaction of the dorsal and tail fin observed in a bluegill sunfish. The presence of the upstream flapping foil increases the performance (thrust and efficiency) of the downstream foil by a significant factor. This provides support for the hypothesis of Drucker and Lauder [14] that the dorsal fin could potentially increase the thrust of the caudal (tail) fin without actively participating in the thrust generation. Numerical simulations also allow us to determine the mechanism responsible for this performance enhancement. It is found that vortex structures shed by the upstream fin increase the effective angle-of-attack of the flow seen by the tail-fin and initiate the formation of a strong LE stall vortex on the downstream fin. This stall vortex convects down the surface of the foil and the low pressure associated with this vortex increases the thrust on the downstream foil. The phase lag between the two foils is the key parameter that determines the extent of thrust enhancement. For this particular configuration, the highest performance enhancement is found when the downstream fin motion lags that of the upstream fin by about $48°$. The current study therefore strongly suggests the presence of a unique vorticity control mechanism in fish propulsion that has not been identified before. It remains to be seen if similar mechanisms can be found in other fish species and swimming animals. Notwithstanding this, the study points the way to a bio-inspired tandem flapping foil combination that could potentially be employed in underwater vehicles for thrust and efficiency augmentation.

The current simulations do not include two effects that could potentially have an impact on fin-fin interactions. The first is the effect of three-dimensionality on the flow. Three-dimensionality of the flow produced by the dorsal fin could affect the evolution of the vortices that interact with the tail-fin, especially since tip vortices from the dorsal fin are known to be convected downstream and interact with the tail fin [25]. Furthermore, the low aspect-ratio delta-wing type shape of the tail-fin could also lead to three-dimensional effects which are not captured in the current study. The second point concerns fin flexibility, which is an important aspect of fish fin function [26,27]. Flexibility is evident in both the dorsal and tail fins from high-speed videos of these fins during locomotion, but is not accounted for in the current simulations. Flexibility leads to slight cambering of the fins and this could potentially alter the flow over the fins by increasing the effective angle of attack and promoting flow separation. Thus, future studies that examine these effects are recommended. Such studies should also investigate the effect of parameters such as foil distance, foil amplitude and frequency since these could potentially have a significant effect on the performance of the tandem foil configuration.

References

1. Long, J.H., Joseph, S., Nicholas, L., Mathieu, K.: Four flippers or two? Tetrapodal swimming with an aquatic robot. Bioinspirat. Biomimet. **1**, 20–29 (2006)
2. Triantafyllou, G.S., Triantafyllou, M.S., Grosenbaugh, M.A.: Optimal thrust development in oscillating foils with application to fish propulsion. J. Fluids Structures **7**, 205–224 (2003)
3. Anderson, J.M., Kerrebrock, P.A.: The vorticity control unmanned undersea vehicle (VCUUV)—An autonomous vehicle employing fish swimming propulsion and maneuvering. In: Proceedings of 10th International Symposium Unmanned Untethered Submersible Technology, NH, 189–195 (1997)
4. Knoller, R.: Die Gesetze des Luftwiderstandes. Flug -Und Motortechnik(Wien) **3**(21), 1–7 (1909)
5. Betz, A.: Ein Beitrag zur Erklarung des Segelfluges. Zeitschrift Fur Flugtechnik Und Motorluftschiffart **3**, 269–272 (1912)
6. Jones, K.D., Dohring, C.M., Platzer, M.F.: Experimental and computational investigation of the Knoller Betz effect. Am. Inst. Aeronaut. Astronaut. J. **36**(7), 1240–1246 (1998)
7. Lighthill, M.J.: Mathematical Biofluiddynamics. Philadelphia: Society for Industrial and Applied Mathematics (1975)
8. Wu, T.: Hydrodynamics of swimming fishes and cetaceans. Advanced Appl Math **11**, 1–63 (1971)
9. Yates, G.T.: Hydrodynamics of body and caudal fin propulsion. In: Webb, P.W., Weihs, D. (eds.) Fish Biomechanics, pp. 177–213. Praeger, New York (1983)
10. Weihs, D.: Design features and mechanics of axial locomotion in fish. Am. Zool. **29**, 151–160 (1989)
11. Gopalkrishnan, R., Triantafyllou, M.S., Triantafyllou, G.S., Barrett, D.S.: Active vorticity control in a shear flow using a flapping foil. J. Fluid Mech. **274**, 1–21 (1994)

12. Tuncer, I.H., Platzer, M.F.: Thrust generation due to airfoil flapping. Am. Insit. Aeronaut. Astronaut. J. **34**(2), 324–331 (1996)
13. Liao, J.C., Beal, D.N., Lauder, G.V., Triantafyllou, M.S.: The Karman gait: novel body kinematics of rainbow trout swimming in a vortex street. J. Exp. Biol. **206**, 1059–1073 (2003)
14. Drucker, E.G., Lauder, G.V.: Locomotor forces on a swimming fish: three-dimensional vortex wake dynamics quantified using digital particle image velocimetry. J. Exp. Biol. **202**, 2393–2412 (1999)
15. Drucker, E.G., Lauder, G.V.: A hydrodynamic analysis of fish swimming speed: wake structure and locomotor force in slow and fast labriform swimmers. J. Exp. Biol. **203**, 2379–2393 (2000)
16. Drucker, E.G., Lauder, G.V.: Locomotor function of the dorsal fin in teleost fishes: experimental analysis of wake forces in sunfish. J. Exp. Biol. **204**, 2943–58 (2001)
17. Udaykumar, H.S., Mittal, R., Shyy, W.: Computation of solid liquid phase fronts in the sharp interface limit on fixed grids. J. Comput. Phys. **153**, 535 (1999)
18. Ye, T., Mittal, R., UdayKumar, H.S., Shyy, W.: An accurate Cartesian grid method for viscous incompressible flows with complex immersed boundaries. J. Comput. Phys. **156**, 209–240 (1999)
19. Scardovelli, R., Zaleski, S.: Direct numerical simulation of free surface and internal flow. Ann. Rev. Fluid Mech. **31**, 567 (1999)
20. Mittal, R., Iaccarino, G.: Immersed boundary methods. Ann. Rev. Fluid Mech. **37**, 239–61 (2005)
21. Triantafyllou, G.S., Triantafyllou, M.S., Streitlien, K.: Efficient foil propulsion through vortex control. Am. Insit. Aeronaut. Astronaut. J. **34**(11), 2315–2319 (1996)
22. Akhtar, I.: Thrust augmentation through active flow control-lesson from a bluegill sunfish. MS Thesis, The George Washington University, Washington, DC, USA (2003)
23. Jayne, B.C., Lozada, A., Lauder, G.V.: Function of the dorsal fin in Bluegill Sunfish: motor patterns during four locomotor behaviors. J. Morphol. **228**, 307–326 (1996)
24. Lauder, G.V.: Caudal fin locomotion in ray-finned fishes: historical and functional analysis. Am. Zool. **29**, 85–102 (1989)
25. Tytell, E.D.: Median fin function in bluegill sunfish, Lepomis macrochirus: streamwise vortex structure during steady swimming. J. Exp. Biol. **209**, 1516–1534 (2006)
26. Lauder, G.V., Madden, P.G.A., Mittal, R., Dong, H., Bozkurttas, M.: Locomotion with flexible propulsors I: experimental analysis of pectoral fin swimming in sunfish. Bioinspirat. Biomimet. (in press)
27. Mittal, R., Dong, H., Bozkurttas, M., Lauder, G.V., Madden, P.G.A.: Locomotion with flexible propulsors II: computational modeling and analysis of pectoral fin swimming in a sunfish. Bioinspirat. Biomimet. (in press)
28. Isogai, K., Shinmoto, Y., Watanabe, Y.: Effects of dynamic stall on propulsive efficiency and thrust of flapping airfoil. Am. Insit. Aeronaut. Astronaut. J. **37**(10), 1145–1151 (1999)
29. Ramamurti, R., Sandberg, W.C., Löhner, R.: Simulation of flow about flapping airfoils using a finite element incompressible flowsolver. Am. Inst. Aeronaut. Astronaut. J. **39**(2), 253–260 (2001)
30. Mittal, R.: Computational modeling in biohydrodynamics: trends, challenges, and recent advances. IEEE J. Oceanic Eng. **29**, 595–604 (2004)